Application of compressed sensing using chirp encoded 3D GRE and MPRAGE sequences

Kamlesh Pawar[1,2] Gary F. Egan[1,2], Zhaolin Chen[1], Jingxin Zhang[3], N. Jon Shah[1,4]

Abstract

An implementation of Non-Fourier chirp-encoding in 3D Gradient Recalled Echo (GRE), susceptibility-weighted imaging (SWI) and Magnetization Pre-pared Rapid Gradient Echo (MPRAGE) sequences is presented with compres-sive sensing reconstruction. 3D GRE and MPRAGE sequences were designed, in which the phase encoding (PE) direction was encoded with spatially selec-tive chirp encoding Radio Frequency (RF) pulses, while the slice and the read-out directions were Fourier encoded using gradients. During each excitation along the PE direction, a different spatially-selective RF excitation pulse was used to encode the PE direction with a complete set of unitary chirp encoding basis. Multichannel compressive sensing reconstruction on the undersampled in vivo data demonstrated that images reconstructed from chirp encoded data were able to preserve the spatial resolution better than the Fourier encoding.

The mean Structural Similarity (SSIM) across five subjects at the acceleration factor of 6, for chirp encoded MPRAGE was 0.934 compared to 0.912 for Fourier encoded MPRAGE. The implementation of prospective undersampling demonstrated the feasibility of using chirp encoding in clinical practice for accelerated imaging. The minimum intensity projection of the compressive sensing (CS) reconstructed susceptibility weighted images revealed that chirp encoding is able to delineate small vessels better than the Fourier encoding with the SSIM of 0.960 for chirp encoding compared to the SSIM of 0.949 for the Fourier encoding. Improved performance of chirp encoding for CS reconstruction and SWI, along with the feasibility of implementation makes them a practical candidate for clinical MRI scans.

Keywords
compressed sensing, image reconstruction, MRI pulse sequence

1. Introduction

Data acquisition in magnetic resonance imaging[1] consists of three processes. The first is an excitation by an Radio Frequency (RF) pulse typically being a constant excitation of the field-of-view (FOV), followed by an encoding—typically Fourier encoding which is achieved by the imaging gradients, and thirdly data acquisition by an analog-to-digital converter. In fact, a spatially selective RF pulse can also be used to perform excitation and encoding simultaneously.[2,3] Early realiza-tion of such an encoding scheme was Hadamard encoding4 which was aimed at improving Signal to Noise Ratio (SNR). Other implementations of such an encoding scheme were Wavelet encoding[5] and singular value decomposition encoding[6,7] that were aimed at accelerated magnetic resonance (MR) imaging.

Accelerated imaging largely benefited from Parallel imaging techniques,[8,9] which have been combined with non-Fourier encoding.10 Compressive sensing (CS) MRI[11,12] is another acceleration technique that exploits the knowl-edge of sparsity, to reconstruct an image from the undersampled k-space data. In order to accelerate MR imaging, a combination of CS and Non-Fourier encoding have been explored in the form of chirp encoding,[13] random encoding[14-16] and noiselet encoding.[17]

Implementation and analysis of chirp encoding for 2D imaging have been demonstrated in Refs.[18, 19]. With the aim of reducing field inhomogeneity artifacts, in Refs. 18-21 chirp encoding was demonstrated for the turbo spin echo sequence. An alternative implementation of chirp encoding was demonstrated in Ref. 13 based on the modification of second order shim coefficients on a 7T scanner.

However, as pointed by the authors, this implementation is not ideal as it causes distortion of the original object, and thus a better implementation is to use chirp modulated RF pulses and dedicated coils. The non-Fourier encoding schemes[3,5,10,14,17] which used modulated RF pulses were implemented in the spin echo sequence with the small flip angle approximation. This implementation is suboptimal in terms of SNR as 90º is an optimal flip angle for the conventional spin echo sequence. In this paper, we present a novel implementation of chirp encoding for 3D Gradient Recalled Echo (GRE) and Magnetization Prepared Rapid Gradient Echo (MPRAGE) sequences and evaluate its performance or accelerated CS reconstruction. Since non-Fourier encoding in spin echo sequence does not utilize all the available SNR, our implementation of non-Fourier chirp encoding in 3D GRE and MPRAGE sequences can be considered a better way of exploiting the advantages provided by non-Fourier encoding schemes for accelerated acquisition. In this work, we show the implementation of chirp encoding using multiple spatially selective RF pulses and demonstrate the application of chirp encoding for accelerated imaging. Unlike Ref. 13, our implementation does not require access to the shim coils and is able to spread the energy in the measurement domain to improve the incoherence required for CS reconstruction. We compare the performance of multi-channel CS reconstruction of chirp encoding and Fourier encoding for retrospectively and prospectively undersampled in vivo datasets. We also demonstrate the application of CS chirp encoding to susceptibility weighted imaging (SWI)[22] and showed that chirp encoding provides better delineation of veins in susceptibility weighted images.

[1]Monash Biomedical Imaging, Monash University, Melbourne, Australia
[2]School of Psychological Sciences, Monash University, Melbourne, Australia
[3]School of Software and Electrical Engineering, Swinburne University of Technology, Melbourne, Australia
[4]Institute of Medicine, Research Centre Juelich, Juelich, Germany

Correspondence Kamlesh Pawar, Monash Biomedical Imaging, Monash University, 770 Blackburn Road, Notting Hill, VIC 3168, Australia. Email: kamlesh.pawar@monash.edu

2. Introduction

2.1 Chirp encoded 3D GRE/MPRAGE pulse sequence design

The pulse sequence presented here (as shown in Figure 1) is a variation of the 3D GRE sequence in which the primary phase encoding (PE) direction is encoded with the complete set of chirp modulated Fourier basis (CMFB) functions. In order to encode the primary PE direction with CMFB, the RF pulses are applied along with gradient in the PE direction. The gradient strength required along the PE direction is given by

$$G_y = \frac{1}{\gamma FOV_{pe} \Delta t_p} \quad (1)$$

where γ is the gyromagnetic ratio, FOV_{pe} is the field-of-view in PE direction, Gγ is the gradient strength in the PE direcJtion and Δt_p is the dwell time of the RF pulse which is defined as Δt_p = (duration of RF pulse)/(number of points in RF pulse). Equation (1) is used to calculate the gradient strength G_γ required in the PE direction during execution of the RF excitation pulse. The FOV_{pe} should be greater than the size of the object in order to avoid aliasing in the PE direction.

The chirp-encoded (CE) MPRAGE sequence was also developed using a similar strategy as for the 3D CE GRE sequence. For the MPRAGE sequence, the 3D CE GRE sequence was modified by inserting a non-selective inversion RF module, which consists of an 180º RF pulse followed by a spoiler in the slice encoding direction (as shown in Figure 1). In this sequence, after each inversion module, all slice encodes are acquired and the TR is defined as a time between two inversion pulses. For prospective undersampling, only the phase encodes corresponding to apredetermined sampling mask were acquired.

2.2 Chirp encoding RF pulse design

Different RF pulse design methods have been presented in the past including the small flip angle approximation[23] and Shinnar-Le Roux pulse design[24,25]. The small flip angle approximation method is mostly used in practice due to its simple implementation. In the small flip angle pulse design (<30°), the RF pulse is computed by taking the Fourier transform of the desired excitation profile. In this work, we use the small flip angle approximation method to design a non-Fourier encoding RF pulse that excites a CMFB in the PE direction.

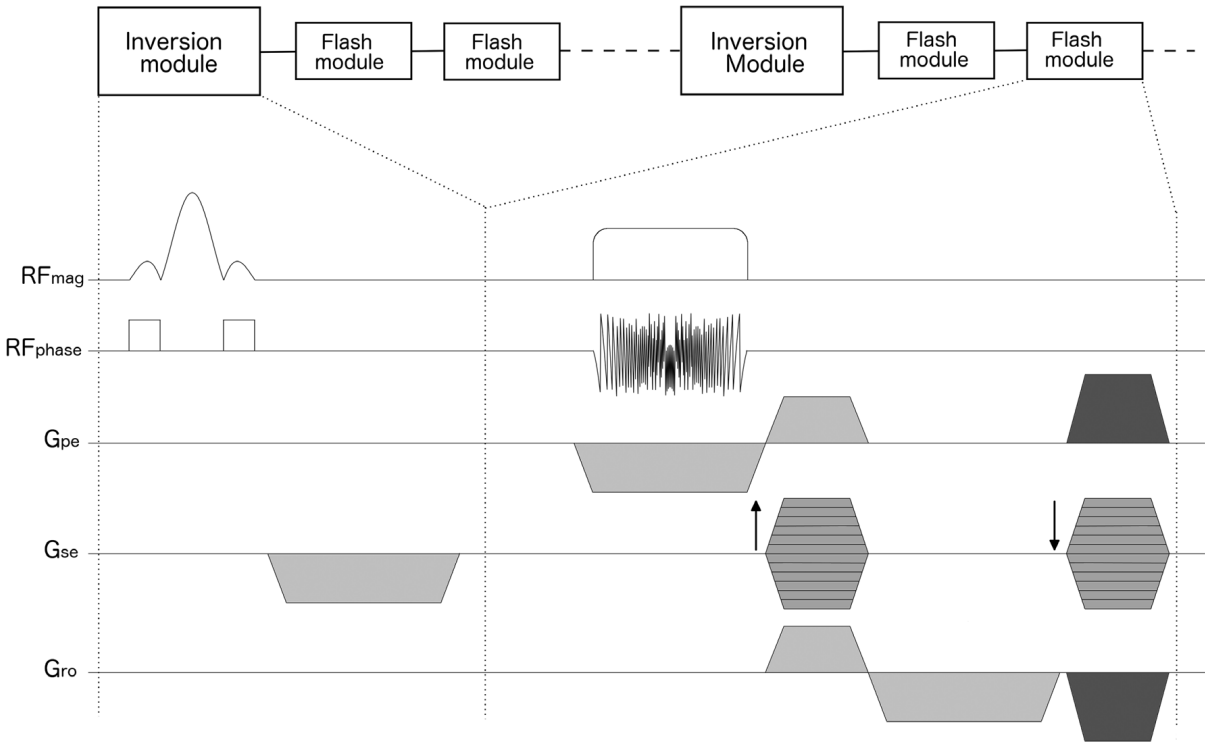

Figure 1: Chirp-encoded 3D MPRAGE sequence; *(G_{se})* Gradient in slice encoding direction; *(G_{pe})* Gradient in phase encoding (PE) direction; *(G_{ro})* Gradient in readout direction. An inversion module is inserted before the FLASH module, consisting of 180° inversion pulse followed by a spoiler in the slice direction. TR is defined as the duration between two inversion modules. The RF pulse along with gradient in PE direction excite the spins and encodes them with a chirp modulated Fourier basis (CMFB) profile; for each PE a different RF pulse is applied; the readout and slice direction are Fourier-encoded using gradients.

In particular, a 3D pulse sequence is introduced to encode the primary PE direction with the CMFB. The secondary PE and Readout (RO) directions are encoded with the conventional Fourier basis. In order to encode the primary PE direction with the CMFB, each RF excitation pulse is different and is calculated as the Fourier transform of the row elements of the CMFB encoding matrix (Fc). A chirp modulation function is defined as:

$$C(n) = e^{j(\Delta C n^2 + \Delta C)} \quad (2)$$

where n ∈ [0, 1, …, N – 1], N is the total number of PEs and ΔC is the chirping factor that controls the spread of energy in k-space.

The CMFB encoding matrix *(F_c)* is designed by modulating each Fourier basis with a chirp modulation function. If *F* is an *N* × *N* Fourier encoding matrix then a CMFB matrix F_c is defined as:

$$F_c = FC_m \quad (3)$$

where C_m is a chirp modulation matrix defined as *Cm* = diag [C(n)], n ∈ [0, 1, …, N − 1].The Fourier transform of each row elements of the chirp encoding matrix F_c, constitutesa unique RF pulse that is subsequently applied along the primary PE direction during data acquisition. The RF pulse matrix (Pc) where each row represents an RF pulse is defined as:

$$P_c = F_c F^H \quad (4)$$

where the subscript *H* denotes the Hermitian transpose. Data acquisition in 2D MRI can be described as:

$$K = E_{pe} I E_{ro} \quad (5)$$

where *K* is the acquired k-space data matrix, *I* is the desired 2D image matrix, E_{pe} is the encoding matrix in PE direction and E_{ro} is the encoding matrix in RO direction.

In conventional MR data acquisition, E_{pe} and E_{ro} are the Fourier transform matrices in the PE and RO direction respectively. For chirp encoding the E_{pe} matrix is replaced with the CMFB encoding matrix *(F_c)* and the acquired k-space data matrix is given as

$$K = F_c I F^H \quad (5a)$$

2.3 Pulse sequence implementation

The pulse sequence was implemented on a Siemens 3T Skyra scanner (Siemens Healthineers, Erlangen, Germany). The implementation of the chirp encoding pulse sequence is non-conventional and the important aspects of the sequence design are described below: RF pulse implementation: The MR scanners we used have a constraint that a maximum of 128 external RF pulses can be prepared in a single sequence. However, a total of 256 different RF pulses were needed to achieve a spatial resolution of 1 mm in the PE direction. To overcome this problem, the RF pulses were computed offline in MATLAB and the pulses were stored as static data within the sequence software at the time of sequence design. The stored RF data were then loaded and RF power and pulse shape was prepared while actual execution of the sequence.

Readout Oversampling to Avoid Aliasing: The RF pulses in the sequence described in Figure 1 were non-selective and excited the whole object. In order to avoid aliasing along the CE direction, the CE direction can be set to either anterior-posterior (A-P) or left-right (L-R). The head-foot (H-F) direction must be set as the RO direction, which avoids aliasing in the H-F direction using the inherent oversampling of a factor of two in the RO direction.

2.4 Image reconstruction model

The k-space data acquired using a Fourier encoding sequence are reconstructed by applying Fourier transforms along all the three dimensions. The k-space data acquired using a chirp encoding sequence has Fourier encoding in two dimensions with chirp encoding in the third dimension. Image reconstruction for CE data involves, first applying a Fourier transform in the two dimensions followed by applying an inverse chirp trans-form in the third dimension. The inverse chirp transform is performed by multiplying the k-space data by the Hermitian transpose of the encoding matrix (FcH). The reconstruction of a 2D k-space data, where one direction is encoded with CMFB and other with Fourier basis can be described as:

$$I = F_c^H K F \quad (6)$$

where, *I* is the reconstructed image and *K* is the acquired CE k-space data.

Figure 2 shows the model for the image reconstruction from fully sampled data for both Fourier and chirp encoding schemes. A 2D plane of acquired data is shown in Figure 2A, D, for Fourier and chirp encoding respectively. The k-space data is Fourier encoded in both x and y directions for the Fourier encoding sequence (Figure 2A), whereas the k-space data is chirp encoded in the y-direction and Fourier encoded in the x-direction (Figure 2D) for the chirp encoding sequence. The first step is to apply a Fourier transform in the x-direction which results in data shown in Figure 2B, E. The second step involves a Fourier transform in the y-direction for the Fourier encoding scheme, while a chirp-transform in the y-direction for the chirp encoding scheme. The final un-regularized reconstructed images are shown in Figure 2C, F.

2.5 Multi-channel compressive sensing reconstruction

The chirp encoding scheme was evaluated on retro-spectively and prospectively undersampled k-space data, in order to assess its performance in multi-channel compressive sensing reconstruction (18). Considering $X \in C^{N2 \times 1}$ to be a vectorized representation of image $\in C^{N \times N}$, the acquired full k-space data can be represented as:

$$y_k = \Phi S_k X \quad (7)$$

where k ∈ [0, 1, …, $N_{ch} - 1$], Nch is the total number of channels, γ_k is the k-space data acquired by the k^{th} channel, $\Phi \in C^{N2 \times N2}$ is the encoding matrix (Fourier or CMFB) and $S_k \in C^{N2 \times N2}$ is a diagonal matrix of the sensitivity map for the k^{th} channel. The Equation (7) can be written compactly as:

$$Y = EX \quad (8)$$

where, $Y = \left[y_1^T y_2^T ..... y_{N_{ch}}^T \right]^T$ and $E = \left[(\Phi S_1)^T (\Phi S_2)^T ..... (\Phi S_{N_{ch}})^T \right]^T$.

If E_u represents an undersampled encoding matrix then undersampled k-space data Y_u can be represented using Equations (7) and (8) as:

$$Y_u = E_u X \tag{9}$$

where, E_u is formed by replacing Φ in E with Φ_u.

A reconstructed, $\hat{X}$, is obtained from following optimization problem using non-linear conjugate gradient iterations:

$$\min_{\hat{X}} \lambda_1 \left\| \Psi \hat{X} \right\|_{l_1} + \lambda_2 TV\left(\hat{X}\right) + \left\| Y_u - E_u \hat{X} \right\|_{l_2}^2 \tag{10}$$

where, Ψ is the wavelet transform operator, TV is a total variation norm and λ_1, λ_2 are regularization parameters for wavelet and TV penalties, respectively.

The optimal regularization parameter can be different for each encoding scheme. Therefore, we did an empirical search for the best regularization parameter between 0.001 and 0.01, and the parameters that provided the maximum Structural Similarity (SSIM) were used.

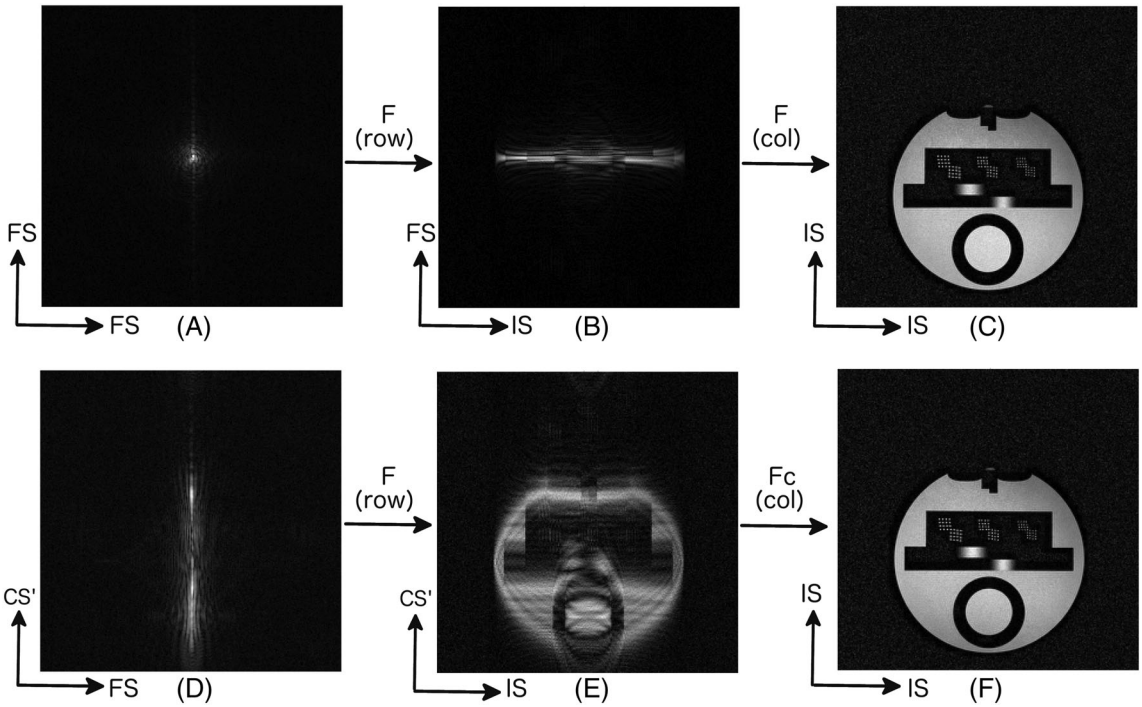

Figure 2: Demonstration of image reconstruction process from acquired Fourier-encoded and chirp-encoded data on a phantom. FS, Fourier space; CS', Chirp space; IS, Image space; F, Fourier transform; Fc, Chirp transform. A-C, demonstrates the image reconstruction in Fourier encoding; A, 2D Fourier encoded k-space data; B, Fourier encoded in the y-direction and image space in the x-direction; C, image reconstructed from Fourier encoded data. D-F, demonstrates the image reconstruction in chirp encoding; D, chirp encoded k-space data with chirp encoding in the y-direction and Fourier encoding in the x-direction; E, chirp encoded in the y-direction and image space in the x-direction; F, image reconstructed from chirp encoded data

2.6 Undersampling scheme

In Fourier encoding the energy is concentrated around the center of k-space, however, in chirp encoding the energy is spread across the phase encodes. Figure 3A, B shows the distribution of energy across the PE (y-direction) for the chirp and Fourier encodings respectively. It can be seen that energy in the chirp domain is spread across the PE, whereas in the Fourier domain the energy is concentrated around the center PE. We found that a simple regular undersampling (Figure 3D) worked reasonably well for the chirp encoding since the "spread of energy" was achieved through the chirp modulation. Hence, we used a regular undersampling pattern for the chirp encoding.

For the Fourier encoding, it is well known that the variable density undersampling (Figure 3E) provides maximal incoherence.[12] Therefore, we used variable density undersampling for Fourier encoding scheme.Figure 3D, E shows the under-sampling pattern used for an acceleration factor of four. The sampling patterns were randomly generated 1000 times and the one with maximal incoherence was selected.

2.7 Receive coil sensitivity map estimation

The sensitivity maps were estimated using the spatially matched filter method described in Ref. 26. The method for 3D sensitivity maps consists of the following steps:

1. Take window of size $k \times k \times k$ around each pixel for all the channels (N_{ch}), resulting in $k \times k \times k \times N_{ch}$ matrix.
2. Reshape the spatial dimension to k^3 to make a $N_{ch} \times k_3$ signal covariance matrix S_b
3. Take the first eigenvector of the matrix $S_b S_b'$, the first eigenvector of size $N_{ch} \times 1$ forms the estimated com-plex sensitivity values at a given pixel for N_{ch} channels.

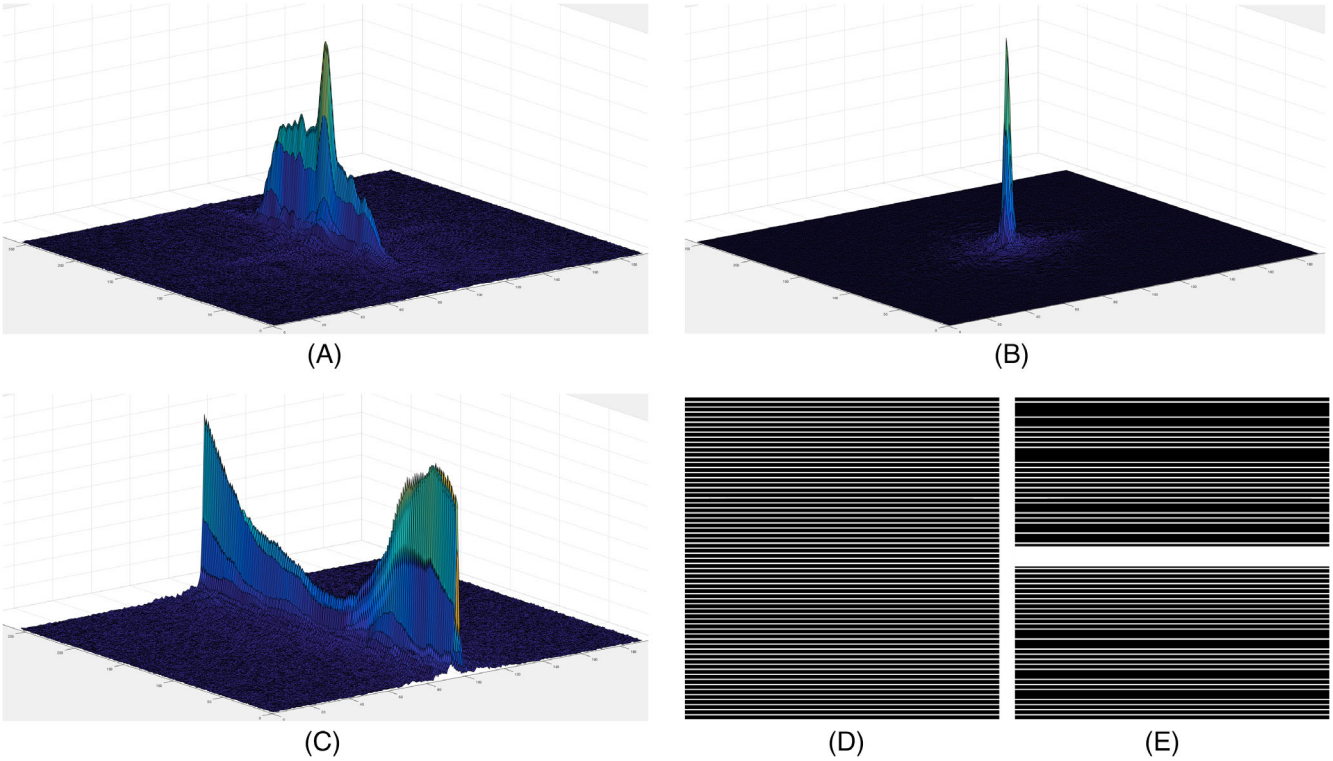

Figure 3 Spread of energy in the measurement domain from the k-space data acquired using 3D GRE sequence; A, C Chirp-encoded k-space where the energy is spread across k-space in the phase encoding (PE) direction. The spread of energy in the measurement domain increases with increasing chirp factor, ΔC = 0.01227 for (A) and ΔC = 0.025 for (C). B, Fourier-encoded k-space where the energy is concentrated at the center of k-space. D, Regular undersampling pattern for chirp encoding. E, variable density undersampling pattern for Fourier encoding [Color figure can be viewed at wileyonlinelibrary.com]

A separate calibration scan was acquired to estimate sensitivity maps. A fast 3D GRE calibration sequence was designed to generate low-resolution images and sensitivity maps were estimated from these low-resolution images. The sequence acquired 64 × 64 × 48 k-space data in 15 seconds with TR = 5 ms. Low-resolution 3D image volume of size 256 × 256 × 192 was reconstructed from 64 × 64 × 48 k-space data with appropriate zero padding in k-space. The sensitivity maps estimated from this calibration scan were used for both Fourier and chirp encoded multichannel compressive sensing reconstruction (MCS) reconstruction.

2.8 Susceptibility weighted image reconstruction

The standard SWI processing was performed on channel combined complex valued MR image obtained from Equation (10) as follows:

1. A low pass filtered image *(I^{LP})* was obtained by multi-plying the Fourier transform of the complex image *(I)* with a 2D Gaussian mask of 256 × 192 and SD 25.
2. A high pass filtered image *(I^{HP})* was obtained as $I^{HP} = I/I^{LP}$
3. The SWI phase mask (g) was obtained from phase (φ) as:

$$g = \begin{cases} \dfrac{\varphi\left(I^{HP}\right)+\pi}{\pi} & \varphi\left(I^{HP}\right) < 0 \\ 1 & \varphi\left(I^{HP}\right) \geq 0 \end{cases}$$

4. The SWI image is thus obtained by multiplying SWI phase with the magnitude of an image *I*.
   $I^{SWI} = g^3\,|I|$

2.9 In vivo data acquisition parameters

In vivo experiments were performed on a Siemens Skyra 3T MRI scanner (Siemens Healthineers, Erlangen, Germany) with a maximum gradient strength of 45 mT/m and a maximum slew rate of 200 mT/m/ms and 32-channel head coil. Informed consent was obtained from volunteers in accordance with the Institution's human research ethics policy. Volunteers were scanned with both the chirp and the Fourier-encoded sequences (3D-GRE and MPRAGE). The chirping factor *(ΔC)* was varied from 0.05 to 0.005 and the factor corresponding to the highest amplitude integral (area under the normalized RF pulse, that is, maximum amplitude of the RF pulse is always one) was selected. The higher amplitude integral of RF pulse implies less RF transmitter voltage required for the desired flip angle. The chirping factor for designing CE RF pulses was ΔC = 0.01227.

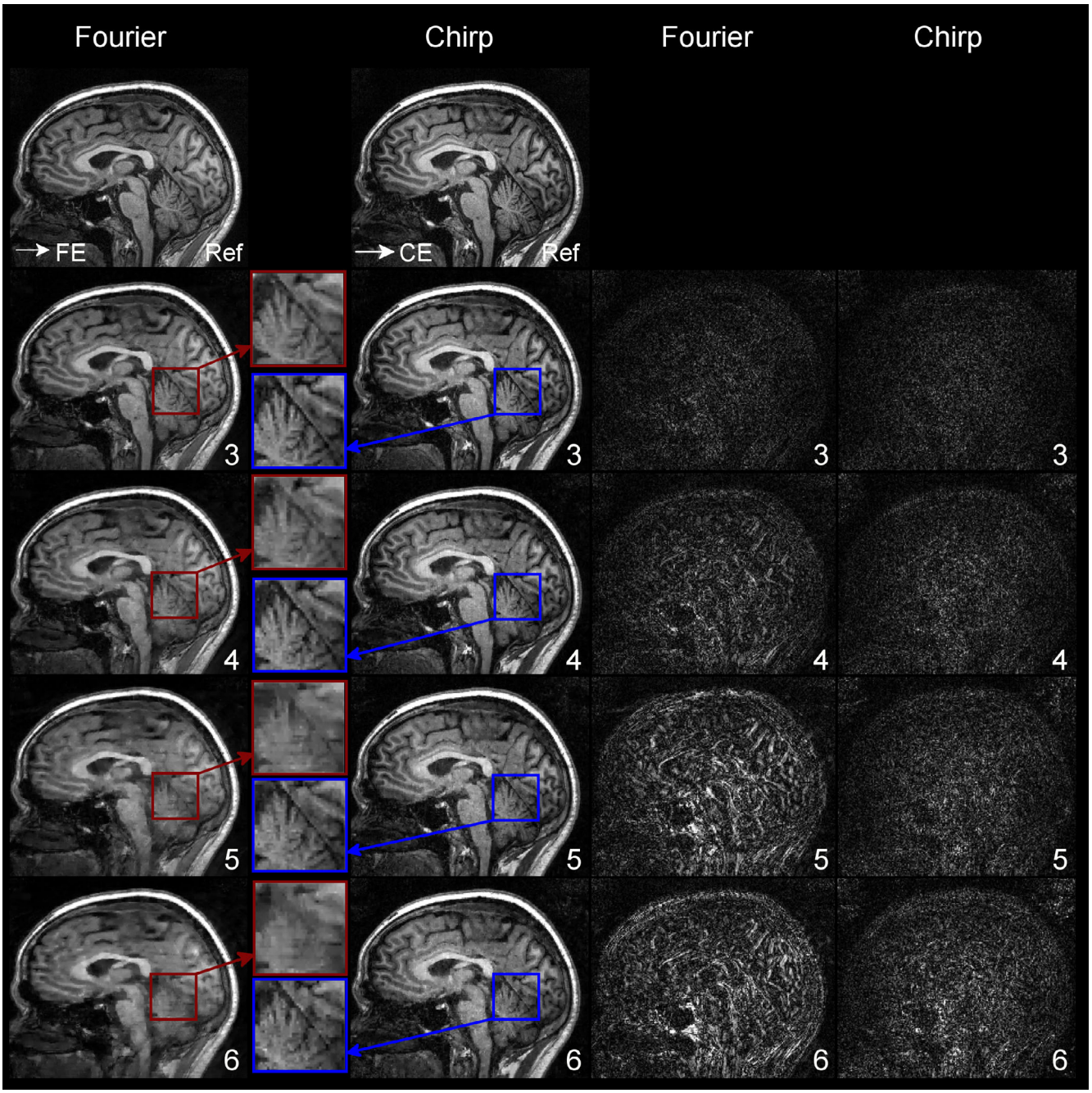

Figure 4 Multichannel compressive sensing reconstruction on the retrospectively sampled Fourier-encoded and chirp-encoded data from MPRAGE sequence where the acceleration factors are given on the bottom-right corner of the panels; Ref: represents the fully sampled reference image; CE: represents the chirp encoding direction. The region of interest inside the bounding box shows that spatial resolution is better preserved using chirp encoding. The error images are shown in the last two columns also show less error in chirp encoding reconstructions [Color figure can be viewed at wileyonlinelibrary.com]

For 3D MPRAGE experiments, five subjects were scanned using a 32-channel head coil: MPRAGE Fourier-encoded data with acceleration factors = 1, 3, 4, 5 and MPRAGE CE data with acceleration factors = 1, 3, 4, 5. For all the scans the protocol consisted of TI = 150 ms, TE/TR = 3.12/2500 ms, flip angle = 10 , FOV = 256 × 256 × 192 mm3, resolution of 1 mm isotropic and total acquisition time for fully sampled scan was 10 minutes 40 seconds.

For 3D-GRE experiments, two fully sampled datasets were acquired, one with Fourier-encoded and another with chirp encoded data for the single subject. The sequence acquisition parameters were: sequence: TE/TR = 5/10 ms, flip angle = 10 , FOV = 256 × 256 × 192 mm^3, resolution of 1 mm isotropic and total acquisition time for fully sampled scan was 8 minutes 10 seconds. An additional 15-second calibration scan with 3D GRE was performed for estimating sensitivity maps for all subjects.

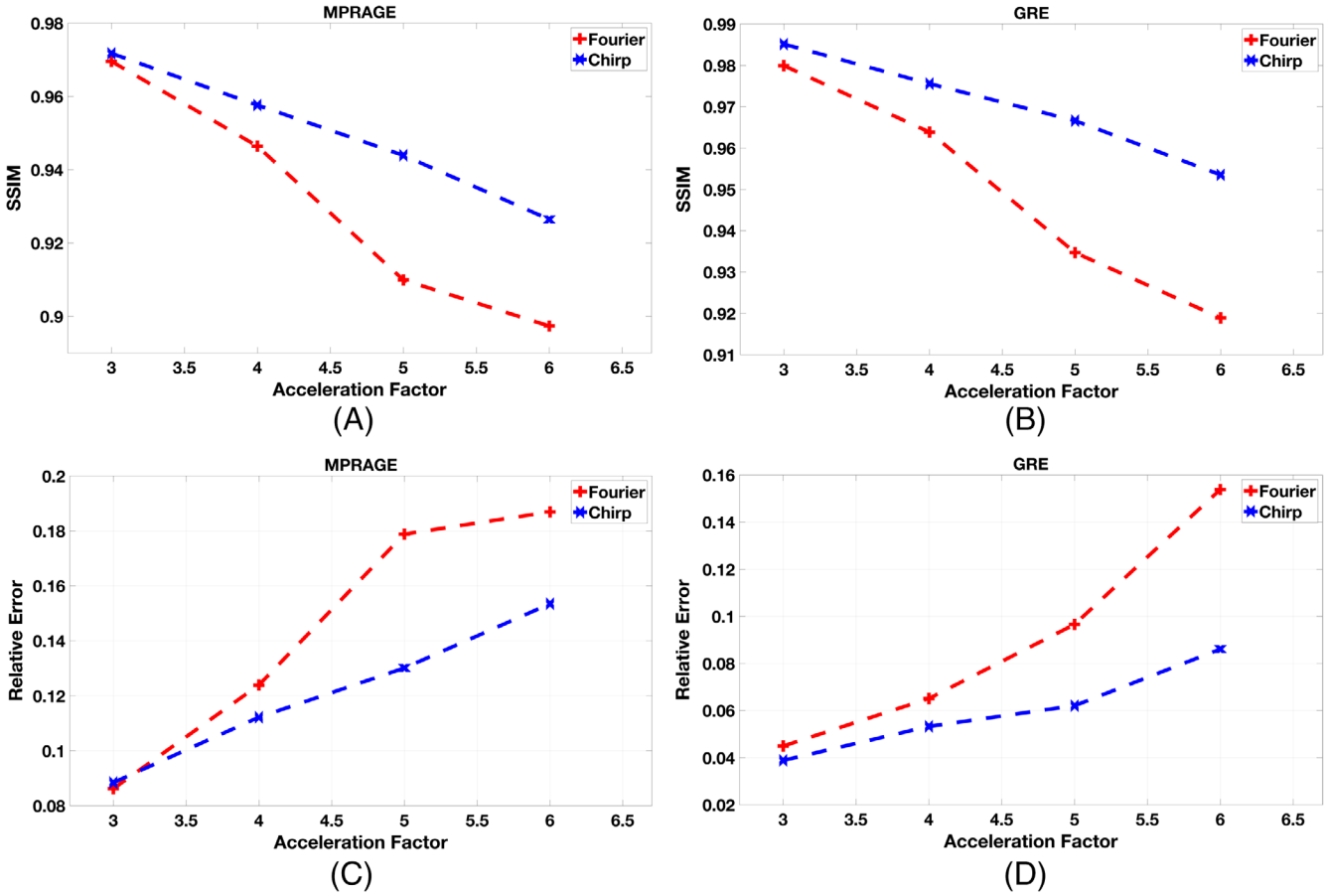

Figure 5 Plots showing the quantitative measures of the image reconstruction quality for one subject. A and B, Structural Similarity (SSIM) for MPRAGE and 3D GRE respectively, higher SSIM signifies better reconstruction; C and D, Relative Error for MPRAGE and 3D GRE respectively, lower Relative Error signifies better reconstruction It is evident from the plots that chirp encoding performed better than the Fourier encoding and the performance difference between the two encodings increases with the acceleration factor [Color figure can be viewed at wileyonlinelibrary.com]

For SWI experiments, twof ully sampled datasets were acquired, one with Fourierencoded and another with chirp encoded data having the same protocol as 3D-GRE except for TE/TR = 20/30 ms. Additionally, for SWI sequence flow compensation gradients were in corporate a long all the three x, y and z directions after each RF pulse.

3. Results

An un-regularized reconstructed image using fully sampled k-space data (Figure 4, Ref images) from chirp encoding was of similar quality as the Fourier-encoded images, having similar noise levels. The Rician noise estimator27 metric was used to compute the noise variance of the normalized (between 0 and 1) reconstructed magnitude images. The noise variance in the normalized 3D image was 1.50% and 1.51% for Fourier-GRE and chirp-GRE respectively. The noise variance in the normalized 3D image was 3.33% and 3.55% for Fourier-MPRAGE and chirp-MPRAGE respectively. This indicates that the chirp encoding is able to provide similar SNR images as the Fourier encoding.

MCS reconstruction after retrospective undersampling by a factor of 3, 4, 5 and 6 are shown in Figure 4 and for the MPRAGE sequence. The reconstructed images from the chirp encoding are able to preserve spatial resolution better than the Fourier encoding. SSIM28 and Relative Error are the two metrics used for quantitative evaluation of reconstructed image quality. Figure 5 shows the SSIM and Relative Error with respect to the acceleration factor for GRE and MPRAGE data acquisition. Both SSIM and Relative Error show improvement in image quality for the chirp encoding. It can be observed from the plots (Figure 5) that chirp encoding performs better in terms of SSIM and Relative error at higher acceleration factors.

The images reconstructed from the retrospective and prospective under sampling by factors of 3, 4and 5are shown in Figure 6.The prospective reconstruction results are consistent with the retro-spective reconstruction demonstrating the feasibility for routine use of the proposed encoding scheme. Small motion between the fully sampled and accelerated scans makes it difficult to compute the quantitative group scores for prospective undersampling. Thus, we computed quantitative group scores across all the subjects for the retrospective undersampling as shown in Figure 7. Both quantitative scores showed better-reconstructed image quality for chirp encoding at higher acceleration factors.

Minimum intensity projection (MIP) across 20 consecutive slices was obtained from the SWI processed images reconstructed with fully sampled and undersampled k-space data (Figure 8).

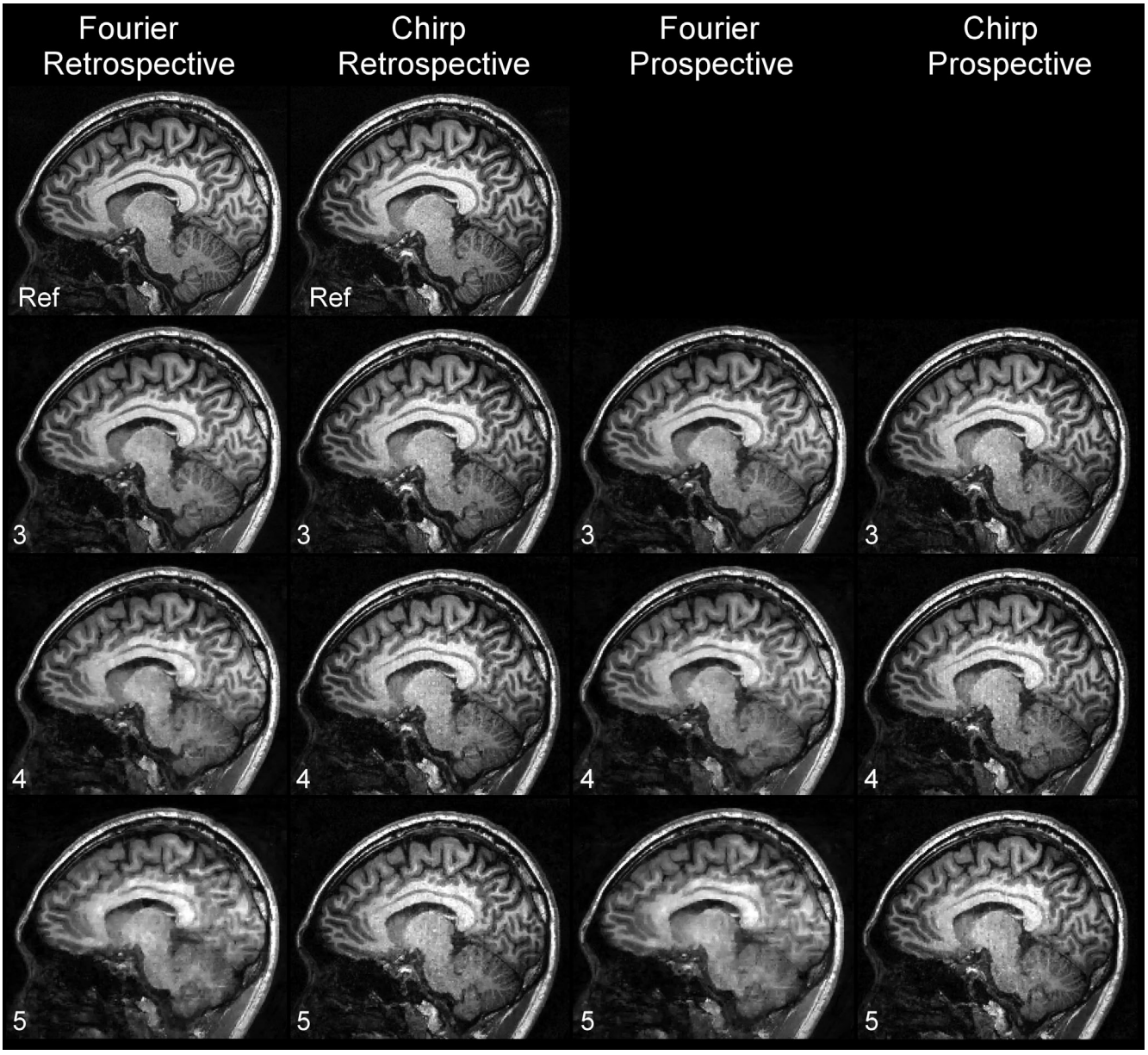

Figure 6: Multichannel compressive sensing reconstruction on the prospectively and retrospectively sampled Fourier-encoded and chirp-encoded data from MPRAGE sequence where the acceleration factors are given on the bottom-left corner of the panels; Ref: represents the fully sampled reference image.

Simple visual inspection reveals that the MIP images from CS reconstructed chirp encoding provides sharper images compared to Fourier encoding. As indicated by blue arrows in Figure 8, the sharpness in the CS reconstructed chirp encoding image is more pro-nounced. The vessels in the cerebral circulation are sharper and delineated well in the chirp encoded images. The improved visual quality is evident from error images (Figure 8 [C, F]) the quantitative scores of structural similarity and relative error. To find the limit of chirp encoding we performed simulation up to an acceleration factor of 9 and calculated peak signal to noise ratio as shown in Figure 9.

4 Discussion

The work presented in this paper is motivated by the fact that non-Fourier encoding schemes demonstrate better performance in compressive sensing reconstruction. Previous works such as spread spectrum,13 random encoding,14 Toeplitz encoding15 and noiselet encoding17 have demonstrated the advantages of using non-Fourier encoding for compressive sensing imaging. Most of the works presented before have implemented the non-Fourier encoding for 2D imaging in spin echo sequences where slice selection was achieved by using an 180 refocusing pulse. The work in Ref. 16 on hybrid encoding presented a 3D acquisition using Toeplitz encoding;

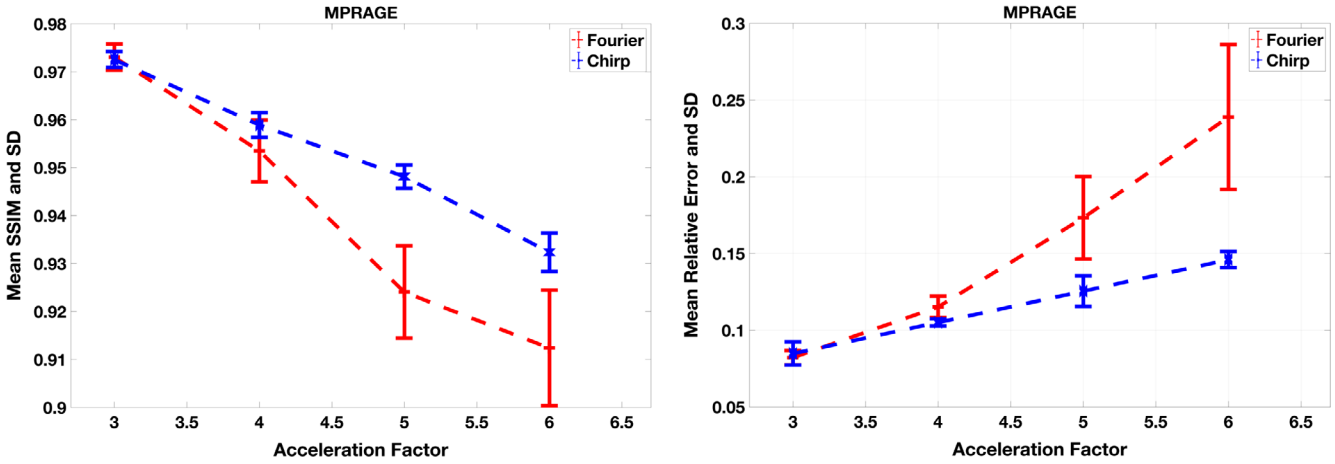

Figure 7: Mean and SD of the Structural Similarity (SSIM) and the Relative error computed across five subjects, both the scores Mean and SD of the Structural Similarity (SSIM) and the Relative error computed across five subjects, both the scores show improvement in chirp encoding reconstruction with the increasing acceleration factor [Color figure can be viewed at wileyonlinelibrary.com]

however, the experiments were only performed on pummelo fruit and were not extended to in vivo imaging. Here we have implemented 3D GRE and MPRAGE sequences and demonstrated that high quality in vivo images with good SNR can be obtained using chirp encoding.

One of the advantages of the proposed chirp encoding implementation is that it does not require modification of the second order shim coefficients, but uses spatially selective RF pulses to realize chirp encoding. In Fourier encoding, gradients are used to encode spins on to the Fourier space. This requires careful implementation of a spoiling scheme to avoid ghosting from the residual transverse magnetization. For instance, in order to maxi-mize the spoiling, the polarity of the spoiling gradient lobe in Fourier encoding needs to be reversed while mov-ing from negative PE to positive PE. However, in chirp encoding, a constant gradient spoiling lobe is enough to avoid ghosting.

Variable density undersampling in Fourier encoding captures the low-frequency components more than the high-frequency components. Insufficient information from the sparsely sampled high-frequency components in Fourier encoding results in loss of resolution in the CS reconstructed images. However, the chirp encoding is able to preserve the resolution better than the Fourier encoding due to the fact that each chirp encode is a linear combination of all the frequency components present in the k-space. Therefore, sufficient high-frequency compo-nents are captured by each chirp encode resulting in bet-ter resolution in the reconstructed images.

One of the limitations of chirp encoding is evident in the simulations (Figure 9) using very high acceleration factors. At the acceleration factor of 9 there is little improvement offered by the chirp encoding. This can be attributed to the fact that at high acceleration factor chirp encoding was not able to capture enough energy. Thus, acceleration factors ranging from 4 to 8 are better suited for the chirp encoding scheme. It is worth noting that at high acceleration factors starting from 6, the reconstructed images for both the chirp and the Fourier encodings were severely degraded, rendering them unusable for clinical purposes. Nevertheless, chirp encoding is still a good candidate for accelerated imaging with intermediate acceleration factors.

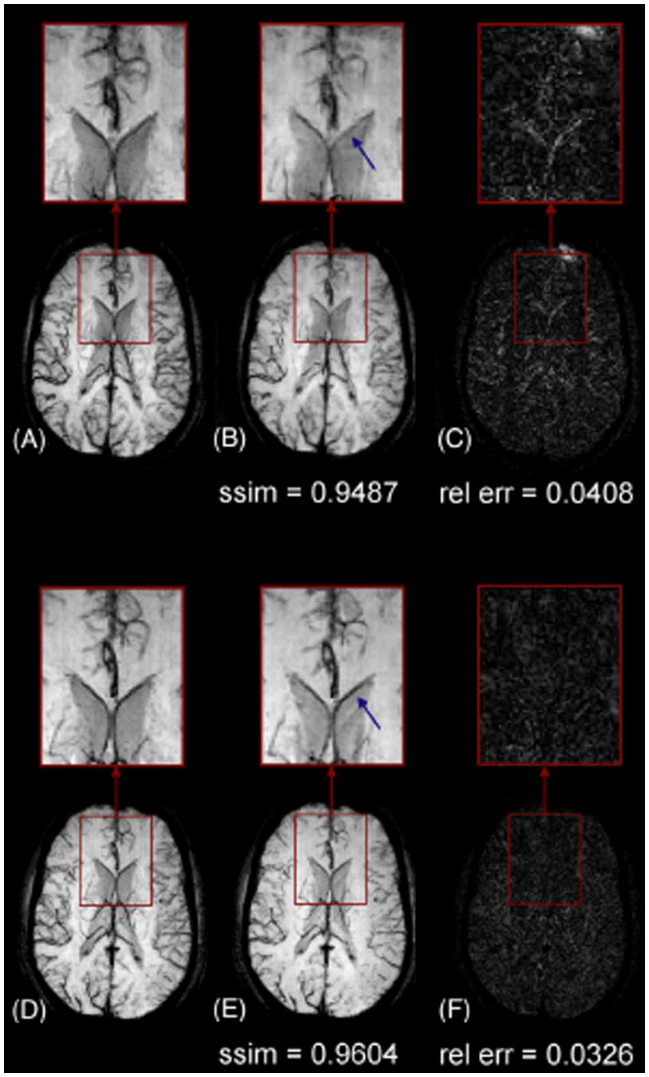

Figure 8: Minimum intensity projection (MIP) across 20 slices of processed susceptibility-weighted imaging (SWI) images; A and D, MIP from Fully sampled Fourier encoded and chirp encoded data respectively; B and E, MIP from undersampled sampled Fourier encoded and chirp encoded data respectively with acceleration factor of 3; C and F, Absolute Error image (scaled by 4×) between fully sampled and undersampled Fourier and chirp reconstructed MIPs respectively. Image. The images reconstructed from chirp encoding is sharper compared to Fourier encoding images as evident from visual inspection (blue arrow, error images) and quantitative scores of SSIM and Relative Error (rel err) [Color figure can be viewed at wileyonlinelibrary.com]

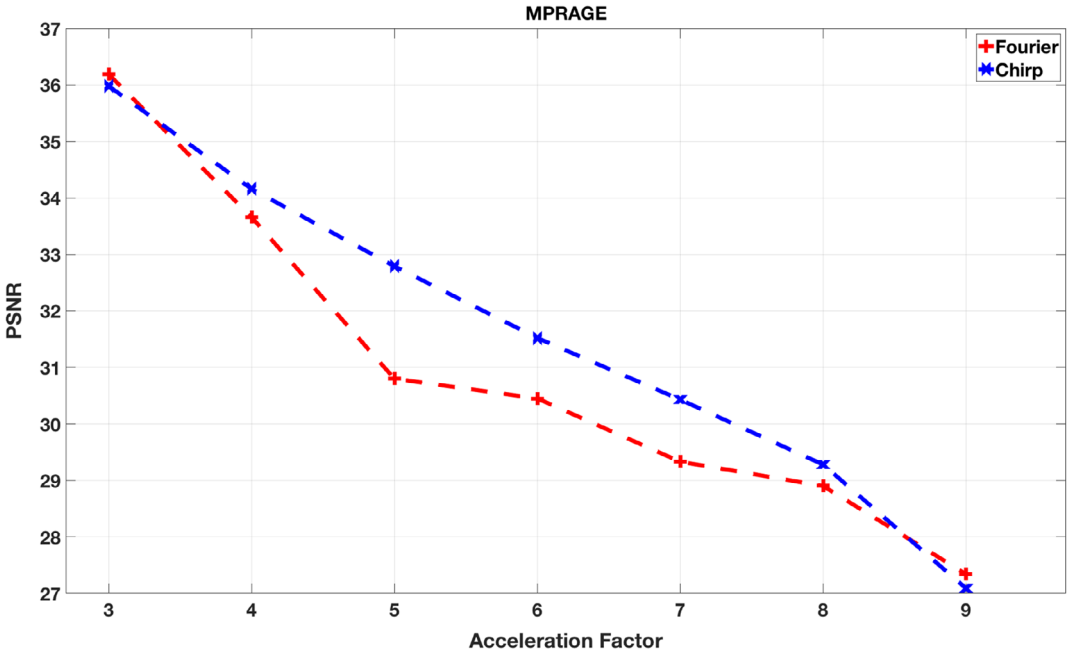

Figure 9: Peak signal to noise (PSNR) plot for Fourier and chirp encoding reconstructions from the acceleration factor of 3 to 9. The figure shows that at the acceleration factors of 4 to 8, chirp encoding performs better than the Fourier encoding [Color figure can be viewed at wileyonlinelibrary.com]

5. Conclusion

Successful implementation of chirp encoding in two frequently used pulse sequences (GRE and MPRAGE) was demonstrated. For fully sampled k-space data, image quality and SNR was comparable to that of Fourier encoding.

The experimental results on prospectively undersampled k-space data showed that the chirp encoding preserves anatomical details better in the images reconstructed using MCS framework. Improved performance of chirp encoding for CS reconstruction and SWI, along with the feasibility of implementation makes them a practical candidate for clinical MRI scans.

6. Acknowledgments

The authors would like to thank the Richard Mcintyre and all the radiographers at Monash Biomedical Imaging, Monash University, Australia for their support in the data acquisition process.

7. Orcid

Kamlesh Pawar https://orcid.org/0000-0001-6199-2312

1. Gupta MP, Shringirishi MM. Implementation of brain tumor segmentation in brain MR images using k-means clustering and fuzzy c-means algorithm. Int J Comput Technol. 2013; 5:54-59.
2. Panych LP. Theoretical comparison of fourier and wavelet encoding in magnetic resonance imaging. IEEE Trans Med Imaging. 1996; 15:141-153.
3. Panych LP, Zientara GP, Jolesz FA. MR image encoding by spatially selective RF excitation: an analysis using linear response models. Int J Imaging Ssyst Technol. 1999; 10:143-150.
4. Weaver JB. Simultaneous multislice acquisition of MR images. Magn Reson Med. 1988; 8:275-284.
5. Panych LP, Zientara GP, Saiviroonporn P, Yoo SS, Jolesz FA. Digital wavelet-encoded MRI: a new wavelet-encoding methodology. J Magn Reson Imaging. 1998;8:1135-1144.
6. Panych LP, Oesterle C, Zientara GP, Hennig J. Implementation of a fast gradient-echo SVD encoding technique for dynamic imaging. Magn Reson Med. 1996;35:554-562.
7. Zientara GP, Panych LP, Jolesz FA. Dynamically adaptive MRI with encoding by singular value decomposition. Magn Reson Med. 1994;32:268-274.
8. Griswold MA, Jakob PM, Heidemann RM, et al. Generalized autocalibrating partially parallel acquisitions (grappa). Magn Reson Med. 2002;47:1202-1210.
9. Pruessmann KP, Weiger M, Scheidegger MB, Boesiger P. Sense: sensitivity encoding for fast MRI. Magn Reson Med. 1999;42: 952-962.
10. Mitsouras D, Hoge WS, Rybicki FJ, Kyriakos WE, Edelman A, Zientara GP. Non-fourier-encoded parallel MRI using multiple receiver coils. Magn Reson Med. 2004; 52:321-328.
11. Donoho DL. Compressed sensing. IEEE Trans Inf Theory. 2006; 52(4):1289-1306.
12. Lustig M, Donoho D, Pauly JM. Sparse MRI: the application of compressed sensing for rapid MR imaging. Magn Reson Med. 2007; 58:1182-1195.
13. Puy G, Marques J, Gruetter R, et al. Spread spectrum magnetic resonance imaging. IEEE Trans Med Imaging. 2011; 31(3): 586-598.
14. Haldar JP, Hernando D, Liang ZP. Compressed-sensing MRI with random encoding. IEEE Trans Med Imaging. 2011; 30: 893-903.
15. Liang D, Xu G, Wang H, King KF, Xu D, Ying L. Toeplitz random encoding MR imaging using compressed sensing. Biomedical Imaging: From Nano to Macro, 2009. ISBI '09. IEEE International Symposium on; Boston, MA, USA; 2009.
16. Wang H, Liang D, King KF, Ying L. Three-dimensional hybrid encoded MRI using compressed sensing. Biomedical Imaging (ISBI), 2012 9th IEEE International Symposium on; Barcelona, Spain; 2012.
17. Pawar K, Egan G, Zhang J. Multichannel compressive sensing MRI using noiselet encoding. PLoS One. 2015;10:e0126386.
18. Pipe JG. Analysis of localized quadratic encoding and reconstruction. Magn Reson Med. 1996;36:137-146.
19. Shrot Y, Frydman L. Spatially encoded NMR and the acquisi-tion of 2d magnetic resonance images within a single scan. J Magn Reson. 2005;172:179-190.
20. Chamberlain R, Park JY, Corum C, et al. Raser: a new ultrafast magnetic resonance imaging method. Magn Reson Med. 2007; 58:794-799.
21. Zhang Z, Lustig M, Frydman L. Phase-encoded xSPEN: a novel high-resolution volumetric alternative to rare MRI. Magn Reson Med. 2018;80:1492-1506.
22. Haacke EM, Xu Y, Cheng YCN, Reichenbach JR. Susceptibility weighted imaging (SWI). Magn Reson Med. 2004;52:612-618.
23. Hoult DI. The solution of the Bloch equations in the presence of a varying b1 field-an approach to selective pulse analysis. J Magn Reson (1969). 1979;35:69-86.
24. Pauly J, Nishimura D, Macovski A, Roux PL. Parameter relations for the shinnar-le roux selective excitation pulse design algorithm. IEEE Trans Med Imaging. 1991;10:53-65.
25. Shinnar M, Bolinger L, Leigh JS. The use of finite impulse response filters in pulse design. Magn Reson Med. 1989;12:81-87.
26. Walsh DO, Gmitro AF, Marcellin MW. Adaptive reconstruction of phased array MR imagery. Magn Reson Med. 2000;43: 682-690.
27. Coupé P, Manjón JV, Gedamu E, Arnold D, Robles M, Collins DL. Robust Rician noise estimation for MR images. Med Image Anal. 2010;14(4):483-493.
28. Wang Z, Bovik AC, Sheikh HR, Simoncelli EP. Image quality assessment: from error visibility to structural similarity. IEEE Trans Image Process. 2004;13:600-612.

How to cite this article:
Pawar K, Chen Z, Zhang J, Shah N J, Egan GF. Application of compressed sensing using chirp encoded 3D GRE and MPRAGE sequences. Int J Imaging Syst Technol. 2020;1–13. https://doi.org/10.1002/ima. 22401